

PAPER REF: 2623

## **EXPERIMENTAL STUDY OF THE CRACK GROWTH OF A CARBON FABRIC REINFORCED PPS UNDER MODE I AND MODE II LOADING CONDITIONS**

**Ives De Baere<sup>(\*)</sup>, Stefan Jacques, Mathias Kersemans, Wim Van Paeppegem, Joris Degrieck**

Department of Materials Science and Engineering, Faculty of Engineering and Architecture, Ghent University.  
Technologiepark-Zwijnaarde 903, B-9052 Zwijnaarde, Belgium.

<sup>(\*)</sup>Email: Ives.DeBaere@UGent.be

### **ABSTRACT**

This manuscript describes an experimental study of both the Mode I and Mode II interlaminar behaviour of a 5-harness satin weave carbon fabric reinforced polyphenylene sulphide (PPS). The mode I crack growth is assessed using the Double Cantilever Beam (DCB) setup and an unstable crack-growth was seen resulting in a saw-tooth like force-displacement curve. Therefore, a model based on Linear Elastic Fracture Mechanics was considered to determine  $G_{IC}$ . The mode II behaviour was studied by the End Notch Flexure (ENF) test where stable crack propagation occurred and the Compliance-Based Beam Method was used to determine the corresponding fracture toughness. As the material showed a peculiar crack growth, especially under Mode I, visual microscopy and ultrasonic C-scans were used to visualise the crack. It could be concluded that the considered approach worked well for this material and reproducible results and values were found.

### **INTRODUCTION**

A delamination or an interlaminar failure is a critical failure mechanism for fibre reinforced composites and, therefore, has already been studied extensively by many researchers, as illustrated in various literature reviews [Sela (1989), de Morais (2004)]. However, it remains an actual research topic, since every day, new polymers with better mechanical properties are being developed for fibre reinforced composites. It was noticed that not that many studies have already been performed on both the Mode I and Mode II crack propagation for a fabric reinforced thermoplastic, as is the subject of the underlying manuscript. Fracasso et al. studied the effect of temperature and strain rate on the values of the Mode I and Mode II fracture toughness [Fracasso (2001)] and a similar study as described here was performed by Zenasni et al [Zenasni (2006)], where an 8-harness satin weave carbon fabric reinforced PEI was considered. Their emphasis, however, was more on comparing different theories for the determination of  $G_{IC}$  and  $G_{IIC}$  and not so much on the crack behaviour. Finally, they only consider crack initiation from the insert, not the crack propagation in the material.

In this manuscript, the emphasis lies on the crack propagation of a fabric reinforced thermoplastic. The Mode I behaviour was investigated with the commonly used Double Cantilever Beam setup, but since the force-displacement curve deviated from the expected form, as discussed in the '*ASTM D5520-01 Standard test method for Mode I interlaminar fracture toughness of unidirectional fiber-reinforced polymer matrix composites*', the value for the Mode I fracture toughness is derived by fitting a model based on Linear Elastic Fracture Mechanics (LEFM) on the experimental results. Furthermore, a microscopic evaluation of the side of the specimen was conducted to investigate the specific jumps during

crack growth and non destructive evaluation using ultrasound was used to determine the shape of the crack front.

The mode II crack growth was investigated using the End Notch Flexure setup and by doing a displacement-controlled test and fulfilling a geometrical demand, stable crack propagation could be achieved. Values for  $G_{IIC}$  were derived using a compliance-based beam method.

## MATERIALS AND METHODS

The composite material used for the experiments was a 5-harness satin weave carbon fabric reinforced polyphenylene sulphide (PPS). The carbon PPS plates were hot pressed at 300°C and 10 bar and one stacking sequence was used for this study, namely  $[(0^\circ, 90^\circ)_{4s}]_s$ . The delamination is manufactured by inserting a Kapton layer of 13  $\mu\text{m}$  thick between the two middle layers before hot pressing.

The in-plane elastic properties and the tensile strength properties are listed in Table 1. This material was supplied to us by Ten Cate Advanced Composites (The Netherlands).

**Table 1** Elastic and strength properties of the CETEX® material

$E_{11}$	$E_{22}$	$\nu_{12}$	$G_{12}$	$X_T$	$\epsilon_{11}^{ult}$	$Y_T$	$\epsilon_{22}^{ult}$	$S_T$
[GPa]	[GPa]	[-]	[GPa]	[MPa]	[-]	[MPa]	[-]	[MPa]
56.0	57.0	0.033	4.175	736	0.011	754.0	0.013	110.0

The test coupons were sawn with a water-cooled diamond saw. Fig. 1 (a) shows the dimensions of the Double Cantilever Beam specimens and Fig. 1 (b) shows the used End Notch Flexure geometry.

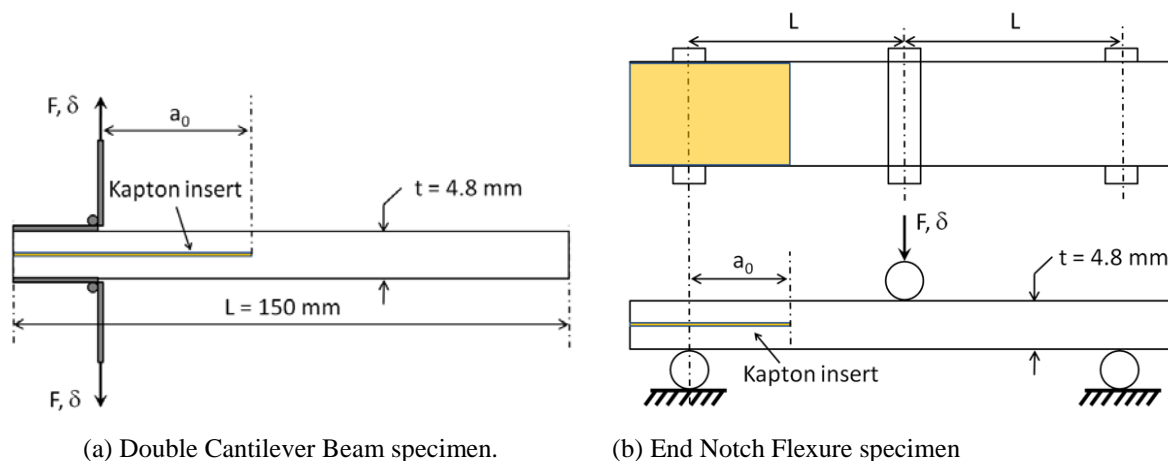


Fig. 1 Dimensions of the used specimens

All mechanical tests were performed on an electromechanical INSTRON 5800R tensile testing machine with a FastTrack 8800 digital controller and a load cell of  $\pm 10\text{kN}$ . The quasi-static tests were displacement-controlled. For the registration of the tensile data, a combination of a National Instruments USB 6251 data acquisition card and the SCB-68 pin shielded connector were used. The load  $F$  and displacement  $\delta$ , given by the FastTrack controller were sampled on the same time basis.

The non destructive evaluation of the specimens was performed using an in-house developed robot, as illustrated in Fig. 2. For the C-scans, a focused broadband shock wave transducer (H5M with  $f = 5\text{MHz}$ ) of the scanning robot was operated in the pulsed regime, using the

USIP40 multi-channel ultrasonic instrument (center frequency  $f = 1 - 30 \text{ MHz}$ ). The coupling medium is water and the measurements shown in this report are recorded in transmission by means of piezo-electric immersion transducers. More details on the experimental setup can be found in [Kersemans (2012)].

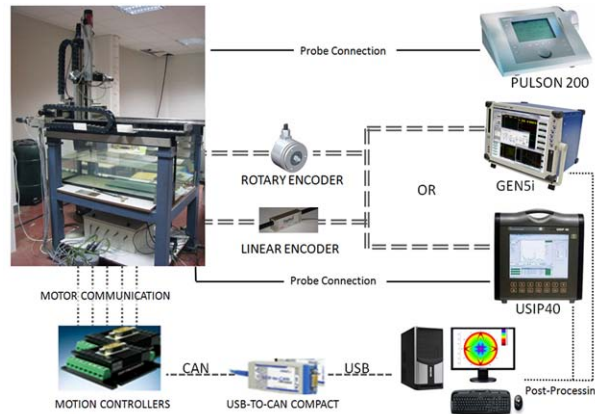


Fig. 2 Experimental setup for the C-scans

## EXPERIMENTS AND DISCUSSIONS

### Mode I Double Cantilever Beam experiments

Because of the high processing temperature, the kapton film stuck to the specimen and as it proved very difficult to open the specimen in such a way that the kapton had released entirely, but without causing any crack growth, it was decided to immediately induce a pre-crack. The pre-crack is induced by opening the specimen at 2 mm/min on the tensile machine until the first crack growth occurs. Next, the specimen is unloaded and the actual crack length is measured using a microscope. Then, the actual test is conducted, also at 2 mm/min, and thus crack growth always starts from a realistic crack, not from the edge of an insert. Table 2 gives the dimensions of the specimens considered here.

Table 2 Dimensions of the used DCB-specimens

Specimen	Width [mm]	$a_0$ before pre-crack [mm]	$a_0$ after pre-crack [mm]
MI-1	22.5	48.3	52.0
MI-2	22.5	48.3	52.7
MI-3	22.5	47.8	55.1
MI-4	21.75	49.7	53.2

Fig. 3 illustrates the results of the first three specimens (MI-1, MI-2 and MI-3) and an unstable saw tooth-like crack propagation can clearly be seen. In [Enasni (2006)], this behaviour can be seen in the force-displacement curves, but only very limited. They are still able to use the characteristic points in the ASTM standard (NL, 5% and  $P_{\max}$ ). Such stick slipping was also reported in [Fracasso (2001)] for a fabric reinforced PEEK, but there emphasis was on the influence of temperature and speed. From Fig. 3, it may be noted that despite the unstable growth, the reproducibility is quite high, both for these experiments and others, not shown here. The initial bending stiffness of specimen MI-2 is higher than for the other specimens, which is in fact unexpected, since the initial delamination length of MI-2 is slightly higher than the others (see Table 2). However, when observing the images taken of the side just after the pre-crack, it was seen that for MI-1, the crack tip is not in the centre of the specimen, contrary to MI-2. As such, there is one adherent thinner than the other for MI-1,

resulting in a lower bending stiffness. The effect of the length of the pre-crack can be seen when comparing MI-3 with MI-1; the pre-crack is roughly 2.5 mm longer for MI-3, the stiffness is significantly little lower.

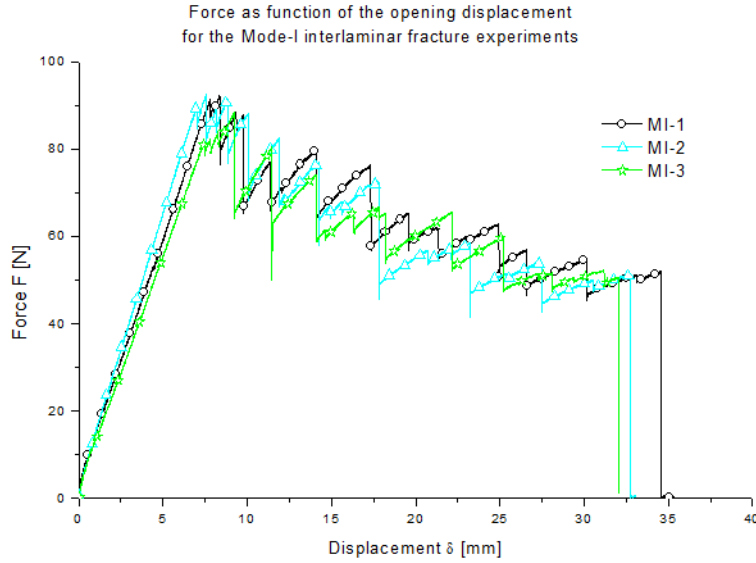


Fig. 3 Force-displacement curve for the DCB tests on all specimens mentioned in this manuscript.

In order to determine the value of  $G_I$ , an analytical model based on linear elastic fracture mechanics is used, as the methodology for determining the value of  $G_{IC}$  given by the ‘*ASTM D5528-01 Standard test method for Mode I interlaminar fracture toughness of unidirectional fiber-reinforced polymer matrix composites*’ cannot be used because (i) the saw-tooth like behaviour and (ii) the absence of the non-linear behaviour in the initial loading slope. The necessary force  $F$  for crack propagation is given by [Turon (2010)]:

$$F = \sqrt{\frac{G_{IC} b^2 h^3 E_{11}}{12a^2}} \quad (1)$$

With  $G_{IC}$  the critical strain energy release rate [N/m]  
 $b$  the width of the specimen [mm]  
 $h$  half the thickness of the specimen [mm]  
 $E_{11}$  Young’s modulus in the warp direction [Pa]  
 $a$  the length of the delamination [mm]

The corresponding displacement  $\delta$  is given by [Turon (2010)]:

$$\delta = F \frac{8a^3}{bh^3 E_{11}} \quad (2)$$

Eliminating the delamination length  $a$  from both equations yields:

$$F = \sqrt{8} \left(\frac{G_{IC}}{12}\right)^{\frac{3}{4}} \frac{1}{\sqrt{8}} b (h^3 E_{11})^{\frac{1}{4}} = f(G_{IC}) \delta^{-0.5} \quad (3)$$

The general idea is to fit Equation 3 on the experimentally derived curves in order to have a value for  $G_{IC}$ , since all other parameters in Equation 3 are known. However, the choice remains on what part of the curve it should be fitted. Since  $G_{IC}$  corresponds with crack growth, it is logical to fit it on the top peaks of each curve, corresponding with the point at which the crack is about to propagate. Fig. 4 shows the best fitting power laws on three of the

mentioned experiments, without taking the exponent of -0.5 into account. It can be seen that the exponent is close but not equal to -0.5.

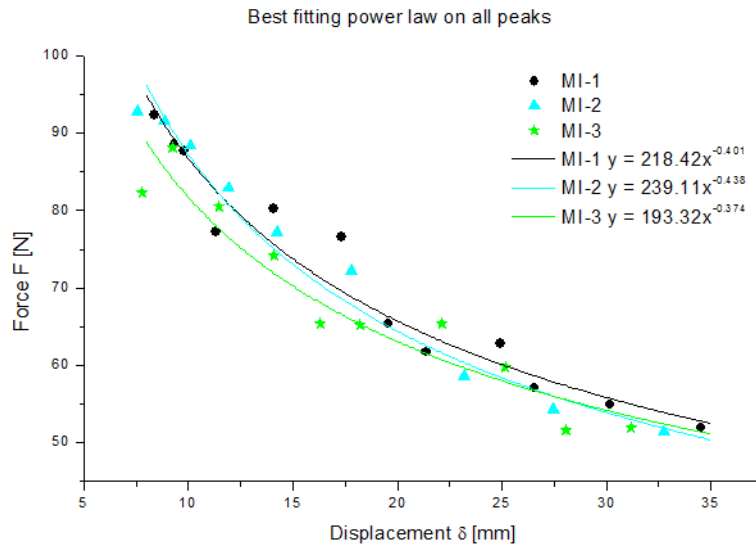


Fig. 4 Illustration of the best fitting power laws on the peaks just before crack propagation

As such, there are two options. The first is fitting Equation 3 through the very first peak, since this is the initiation of the crack. This yields a value for  $G_{IC,initiation}$  but these curves do not capture the behaviour after initiation well. For a given  $\delta$ , the force is always underestimated. Therefore, a second option is considered, namely fitting Equation 3 through all peaks, except the first. This will yield a value for the propagation of the crack,  $G_{IC,propagation}$ . This yields a better approximation for the curves, but it overestimates the force for initiation, meaning the first peak of every curve. Using this approach, an average value of 852 N/m was found for the initiation of a ‘natural’ crack  $G_{IC,initiation}$  and an average value of 970 N/m was derived for the propagation of the crack.

To further investigate the origin of the saw tooth like force-displacement curve and to assess the role of the fabric in this part specimen MI-3 was polished and crack growth was monitored during the experiment using a travelling microscope. Pictures were taken every time the crack propagated, so that the crack jump can be visualised by comparing the successive pictures. It was verified that there was no stable crack propagation in between two teeth of the saw-tooth like force-displacement curve, so the picture just after one crack jump is still relevant to compare with the next jump with respect to the crack tip position.

The load-displacement curve of the experiment is already shown in Fig. 3 and in total 17 pictures were taken to determine the crack behaviour. In general, the following remarks can be made (also see Fig. 5): the crack tip after a jump is either just before or just after two contacting weft ( $90^\circ$ ) fibre bundles. As such, the propagation length on the polished edge is not constant. However, three scenarios are possible, as seen from the polished edge: (i) the crack propagated along an entire unit cell, about 7.4 mm. The crack can start either before a weft bundle, or after a weft bundle, depending on the previous jump (Fig. 5 (a)); (ii) the crack propagates from just after one weft bundle till just before the next, meaning it grows between the warp bundles (Fig. 5 (b)); (iii) the crack propagates along a single weft bundle (Fig. 5 (c)).

Occasionally, meta-delaminations also occur, meaning that a crack travels in the fabric just above the symmetry-plane. In rare cases, the crack propagated very little (less than 0.05 mm) in between two warp bundles, causing a very small decrease in the force.

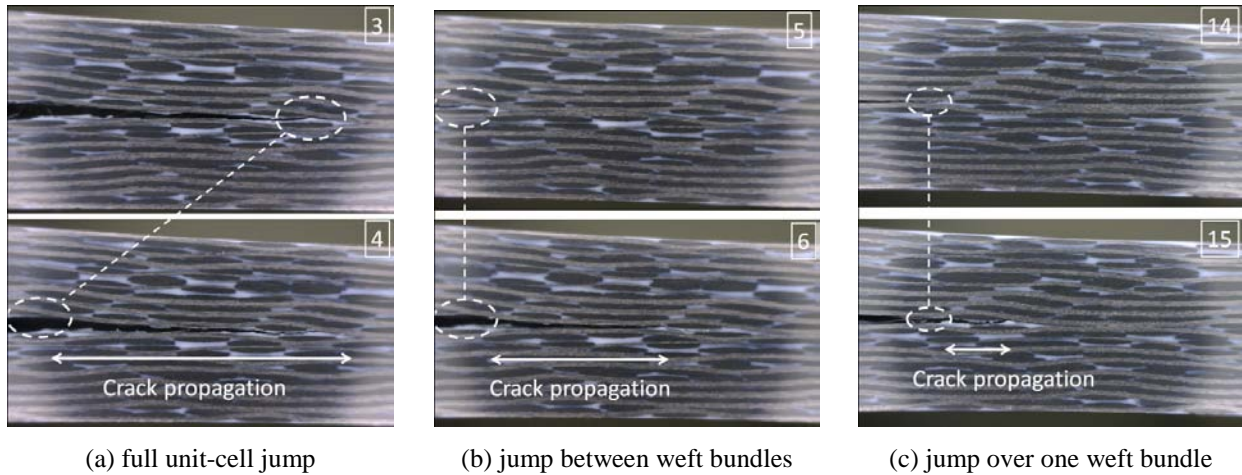


Fig. 5 Overview of the occurring types of crack growth (specimen MI-3)

It was observed that the crack does not show a stable propagation between the warp ( $0^\circ$ ) bundles, although in some cases a small crack was present, resulting from a previous jump. This, however, can be explained by the fact that the weave is a 5-harness, meaning that the local geometry seen on the edge is not the same throughout the width of the specimen, the crossing-over point of weft and warp shifts in the pattern.

To further investigate the propagation and the shape of the crack front, a second type of experiments was conducted: the specimen was again loaded at 2 mm/min until the crack propagated, after which it was unloaded and a C-scan was performed. Fig. 6 illustrates the load-displacement curve of the experiment, which is of course similar to that of MI-1 and MI-2. Furthermore, the analytical prediction (Equation 3) is also plotted for the averaged values of both  $G_{IC,initiation}$  and  $G_{IC,propagation}$  to validate these values. As can be seen, both curves capture the behaviour quite nice. The curve using  $G_{IC,initiation}$  captures the initiation of the crack growth, but then underestimates the peak forces, whereas the curve using  $G_{IC,propagation}$  overestimates crack initiation, but predicts the propagation peaks very well.

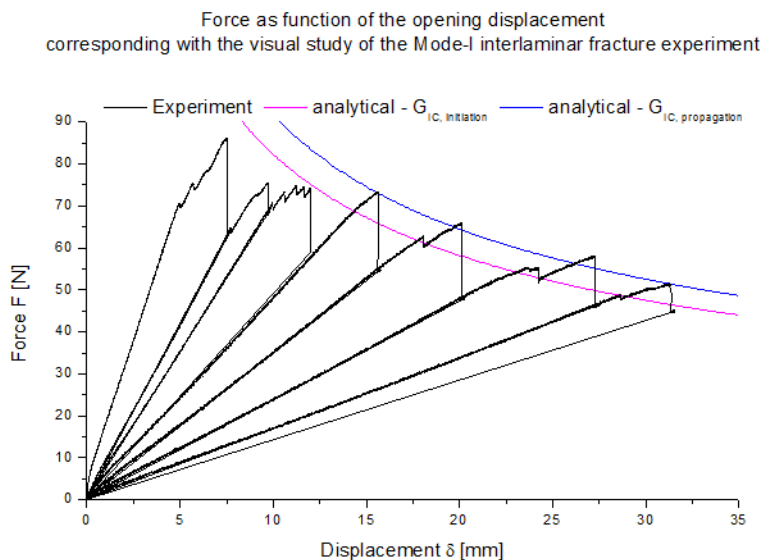


Fig. 6 Force-displacement curve for the DCB test on MI-4, used for the ultrasound investigation

Fig. 7 illustrates the performed C-scans during the experiment on MI-4. During each C-scan, a plastic part was added on the surface of the specimen as a geometrical reference, in order to determine the crack jump; this reference is the blue line on each image. The red line represents the (averaged) crack front. Fig. 7 (a) was performed with a  $0.35 \times 0.35 \text{ mm}^2$  resolution, Fig. 7 (b-h) were done at  $0.3 \times 0.3 \text{ mm}^2$ , which is the highest resolution possible with the provided software. In the images, the crack grows from the bottom up.

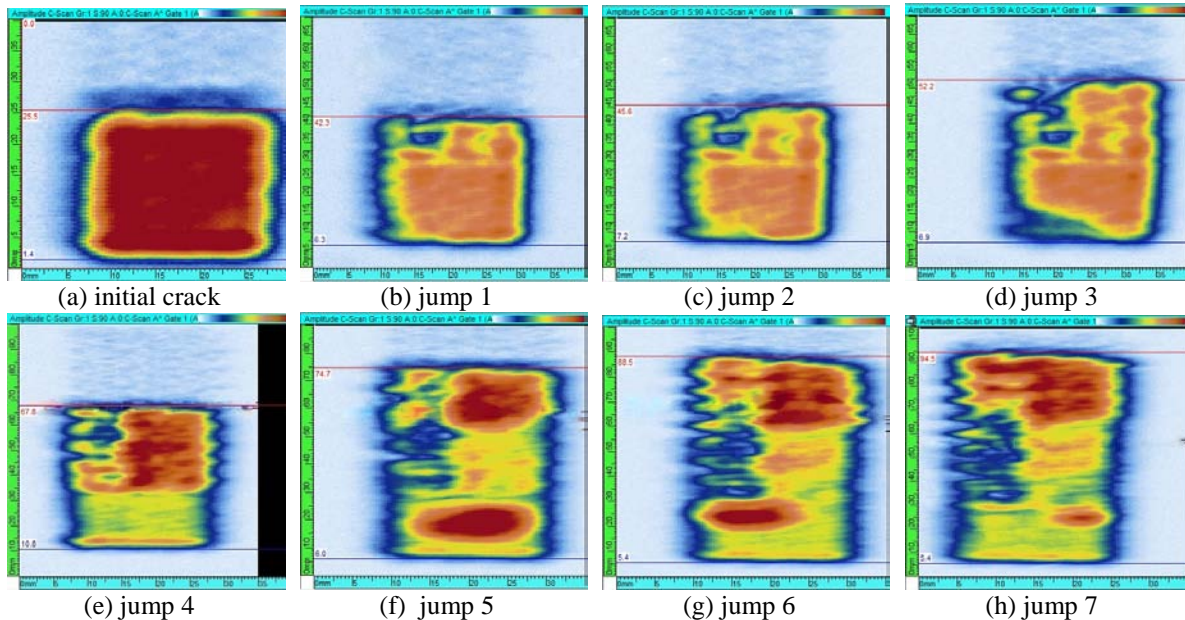


Fig. 7 Overview of the different C-scans performed after each crack jump

Due to the kapton insert, the initial crack front is a fairly straight line (a), but after most jumps, the crack front shows a stepwise trend, rather than a convex or concave shape. Unfortunately, the resolution was still not high enough to determine whether the crack front follows the 5-harness satin pattern. Moreover, the crack front does not always stay perpendicular to the longitudinal axis of the specimen. For instance for jump 2 (c), the left side seems to have progressed 3 mm more than the right side, which is most likely caused by the 5-harness weave pattern. By using the ‘averaged’ crack front and the geometrical reference, the crack propagated over 12.2 mm, 2.4 mm, 6.9 mm, 11.7 mm, 11.7 mm, 14.4 mm and 6 mm for jumps 1 till 7 respectively.

Finally, it can be noticed that in jumps 5, 6 and 7 there is a large blue spot, due to a higher absorbance of the ultrasound. After the test was completed, it was verified by optical analysis of the fracture surface that the crack indeed showed different failure behaviour at that location.

### Mode II End Notch Flexure experiments

The  $G_{IIC}$  can be obtained from the End Notch Flexural test (ENF), meaning simple three-point bending experiments on specimens with an initial delamination, as already illustrated in Fig. 1. The determination of  $G_{IIC}$  is done according to the ‘Compliance-Based Beam Method’, as explained in [Arrese (2010), Srinivasan (2009)]. This method has two important advantages: (i) there is no need to continuously measure the delamination length during the experiment and (ii) this method takes the material degradation just behind the crack tip into account. This method only has one demand with respect to the geometry, namely that  $a_0/L \geq 0.7$ ; this to ensure stable crack growth. Although unexpected considering the unstable crack growth for the double cantilever beam tests, preliminary experiments have shown that stable crack

propagation is indeed achieved using this method for the material under study. As preliminary tests showed the expected behaviour without inducing a pre-crack, contrary to the DCB tests, no pre-crack is considered here.

Table 3 shows an overview of the three specimens illustrated in this manuscript. As can be seen, two different geometries are considered, to illustrate the effect of the geometry on the stable crack-growth and the results.

Table 3 Dimensions of the used ENF-specimens

Specimen	Width [mm]	Half span L [mm]	Crack length $a_0$ [mm]
ENF1	11.4	72.5	55
ENF2	11.5	72.5	55
ENF3	16.1	100.0	70

Fig. 8 shows the corresponding force-displacement curves of the ENF experiments, conducted at a speed of 0.5 mm/min; for comparison purposes, all values have been normalized to a width of 20 mm. These results were also found for other specimens, not illustrated here.

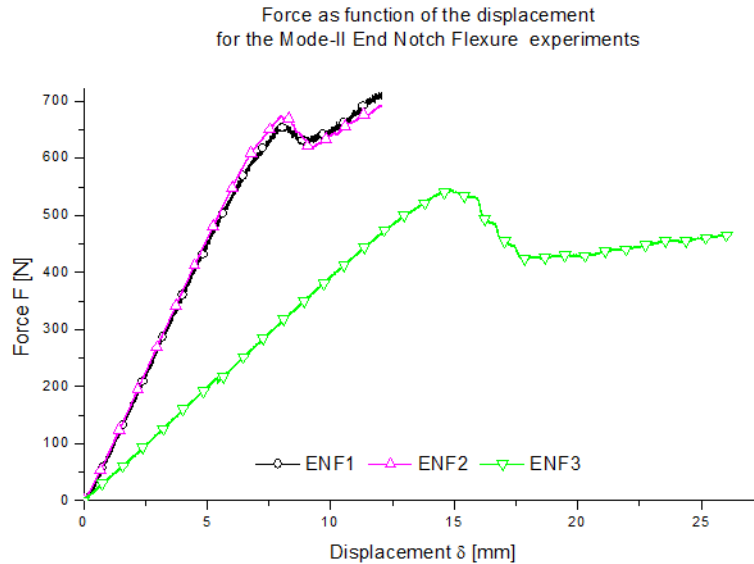


Fig. 8 Force-displacement curve for the ENF tests

First, it should be noted that the expected shape is present. The force increases until the crack initiates and propagates, resulting in a decrease in force. Once the crack has reached the centre of the specimen the force increases again, but with a different slope. It must be noted that the larger specimen shows a significantly larger stage of crack propagation, which will facilitate the determination of  $G_{IIC}$ . Finally, the reproducibility of the results for the same geometry is very high (better than for the Mode I DCB tests), which was also confirmed by other experiments, not shown here. From these experiments, the  $G_{IIC}$  was derived using the approach as described in [Arrese (2010)], yielding the following equation:

$$G_{IIC} = \frac{9F^2 a_{eq}^2}{16b^2 E_f h^3} \text{ with } a_{eq} = \sqrt[3]{\frac{c_{corr}}{c_{0,corr}} a_0^3 + \frac{2}{3} \left( \frac{c_{corr}}{c_{0,corr}} - 1 \right) L^3} \quad (4)$$

With  $F$  = the force at the corresponding point of the force-displacement curve [N]  
 $E_f$  = the flexural stiffness [N/m]  
 $b$  = width of the specimen [m]  
 $h$  = half the height of the specimen [m]  
 $a_0$  = initial length of the delamination [m]  
 $a_{eq}$  = the equivalent delamination length [m]  
 $C_{corr} = C - \frac{3L}{10G_{13}bh}$   
 $C_{0,corr} = C_0 - \frac{3L}{10G_{13}bh}$   
 $L$  = half the span [m]  
 $C_0$  = compliance of the linear part of the force-displacement curve [m/N]  
 $C$  = compliance at the corresponding point of the force-displacement curve [m/N]  
 $G_{13}$  = shear modulus of the material [Pa]

The fact that  $G_{13}$  is necessary for this method is sometimes a problem, but for the material under study, the  $G_{13}$  value is accurately determined by meso-scale modelling [Daggumati (2010)] and is equal to 3048 MPa.

Equation 4 is then plotted as a function of  $\Delta a_{eq} = a_{eq} - a_{eq}^{mean}$ , with  $a_{eq}^{mean}$  the mean value of  $a_{eq}$  where there was no crack growth. This curve normally shows a plateau; the value of this plateau is the value of  $G_{IIC, propagation}$ . The value of  $G_{IIC, initiation}$  can be derived from the intersection of this curve with the vertical axis  $\Delta a_{eq} = 0$ . Fig. 9 shows the results corresponding with the experiments above.

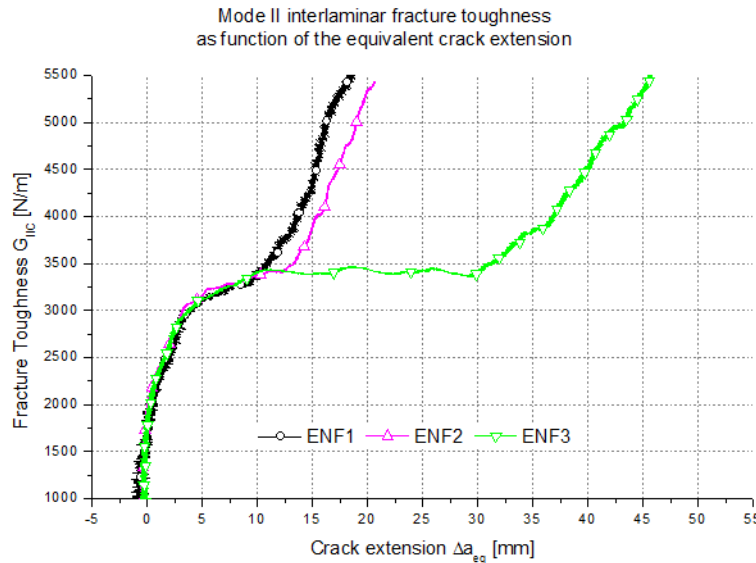


Fig. 9  $G_{IIC}$  as function of  $\Delta a_{eq}$  for the ENF experiments.

First, it should be noted that the correspondence for initiation and stable crack growth is very high. Also, the difference in geometry has a definite influence on the crack propagation, the plateau corresponding with the larger specimens is more pronounced, making it easier to determine the value of  $G_{IIC, propagation}$ . Nevertheless, if the scaling is adjusted only to the curves of ENF1 and ENF2, a sufficiently flat part of the curve, containing a large number of data points (note: only one every 700 points is given a symbol in Fig. 9) is visible. As such, values for  $G_{IIC, propagation}$  can also be derived for these experiments. A value of 1800 N/m was found for  $G_{IIC, initiation}$  and, similar to mode I, a higher value of 3287 N/m for  $G_{IIC, propagation}$ .

Similar to the Mode I assessment, a microscopic study was performed on a polished side of an ENF specimen. Here, it was verified that indeed stable crack propagation occurred, contrary to the DCB-tests. Occasionally, a meta-delamination occurred similar to the Mode I experiments, but since this study revealed no other relevant occurrences, no c-scans were performed for this type of experiment and the microscopic study is not added to this manuscript.

## CONCLUSIONS

This manuscript has studied the interlaminar fracture toughness behaviour of a 5-harness carbon fabric reinforced thermoplastic under Mode I and Mode II loading conditions. To induce the mode I crack propagation, the Double Cantilever Beam (DCB) setup was considered. Because of the nature of the reinforcement, namely the 5-harness fabric, no stable crack propagation was present and a saw-tooth like force-displacement curve was observed. Hence, using an analytical model based on linear elastic fracture mechanics, a curve was plotted on the experimentally derived force-displacement curve. Two values for  $G_{IC}$  were determined, namely one for the initiation of a 'natural' crack  $G_{IC,initiation}$  (average value 852 N/m) and one for the propagation of the crack,  $G_{IC,propagation}$  (average value 970 N/m). The fracture toughness for the propagation starting from the insert was not derived, since in real-life structures, such an insert would not be present. A microscopic study of the crack growth revealed that the jumps in the force-displacement curve were due to the specific 5-harness geometry of the reinforcement. The crack always started and ended either just before or just after a weft ( $90^\circ$ ) bundle and no stable propagation was present when the crack tip was between two neighbouring warp ( $0^\circ$ ) bundles, seen from the side.

In order to induce mode II crack propagation, the End Notch Flexure test (ENF) was used and stable crack propagation was seen. Using the Compliance-Based Beam Method, A value of 1800 N/m was found for  $G_{IIC, initiation}$  and, similar to mode I, a higher value of 3287 N/m for  $G_{IIC, propagation}$ .

With respect to the crack front, the C-scans have shown that the crack front has a stepwise evolution rather than the expected convex or concave shape, but unfortunately, the resolution could not be set high enough to determine whether the crack follows the 5-harness satin weave pattern.

## ACKNOWLEDGMENTS

The authors are highly indebted to the Fund of Scientific Research – Flanders (F.W.O.) for sponsoring this research and Ten Cate Advanced Composites for supplying the material.

## REFERENCES

- Arrese A., Carbajal N., Vargas G. and Mujika F. A new method for determining mode II R-curve by the End-Notched Flexure test. *Engineering Fracture Mechanics* 77(1), pp 51-70 (2010)
- Daggumati S., Van Paepegem, W., Degrieck, J. Xu J., Lomov S.V. and Verpoest I. Local damage in a 5 – harness satin weave composite under static tension: part II - meso – FE modeling. *Composites Science and Technology* 70 (13), pp 1934-1941 (2010)
- de Morais, AB, Rebelo, CC, de Castro, PMST, Marques, AT and Davies, P. Interlaminar fracture studies in Portugal: past, present and future. *Fatigue&Fracture of Engineering Materials & Structures* 27 (9), pp 767-773 (2004)
- Fracasso, R., Rink, M, Pavan, A and Frassine, R. The effects of strain-rate and temperature on the interlaminar fracture toughness of interleaved PEEK/CF composites. *Composites Science and Technology* 61(1), pp 57-63 (2001)
- Kersemans M., Van Paepegem W., Van Nuffel D., Luyckx G., De Baere I., Zastavnik F., Gu J., Sol H., Van Den Abeele K. and Degrieck J. Polar scan technique for material characterization and identification of new operating regimes. *15th International Conference on Experimental Mechanics (ICEM-15)*, 22-27 July 2012, Porto, Portugal
- Sela, N and Ishai, O. Interlaminar fracture-toughness and toughening of laminated composite materials - A review. *Composites* 20 (5), pp 423-435 (1989)
- Srinivasan Sridharan. Delamination behaviour of composites. Cambridge: Woodhead Publishing Limited, Boca Raton: CRC Press LLC. (2008)
- Turon, A. Camanho P.P., Costa J. And Renart J. Accurate simulation of delamination growth under mixed-mode loading using cohesive elements: definition of interlaminar strengths and elastic stiffness. *Composite Structures* 92 (8), pp 1857-1864 (2010)
- Zenasni, R and Saad, BA. Moisture effect on the interlaminar resistance of woven fabric thermoplastic composite. *Journal of Thermoplastic Composite Materials* 19 (6), pp 715-729 (2006)